Structure, melting, and order tendencies of $A_{13}B_{13}$ Lennard-Jones heteroclusters with additive and nonadditive collision diameters

C. Rey and L. J. Gallego
Departamento de Física de la Materia Condensada, Facultad de Física, Universidad de Santiago de Compostela, Santiago de Compostela, Spain
(Received 24 March 1994; revised manuscript received 3 October 1994)

Using constant-energy molecular-dynamics simulations, we studied the lowest-energy structures, melting behavior, and ordering tendencies of $A_{13}B_{13}$ Lennard-Jones (LJ) clusters with additive and nonadditive collision diameters. We found that nonadditivity can significantly affect the properties of the LJ clusters. In particular, small negative nonadditivities give rise to nonicosahedral configurations.

I. INTRODUCTION

The structural and dynamical properties of one-component Lennard-Jones (LJ) clusters have been extensively investigated by molecular-dynamics (MD) and Monte Carlo (MC) simulations (see, e.g., Refs. 1–5). Considerably less attention has been devoted to LJ clusters containing more than one species of atom (heteroclusters), although some work on binary clusters has been published. For instance, MD simulations have been used by Garzón *et al.*[6] to investigate the lowest-energy structures, impurity solvation, and melting of $A_{12}B$, $A_{13}B$, $A_{55}B$, and $A_{13}B_{13}$ LJ clusters for various values of the relative atomic size and interaction strength. The melting behavior of $A_{12}B$ LJ clusters has also been studied by Grimson[7] using MC simulations. More recently, Clarke *et al.*[8] have performed MC and MD simulations to analyze the structure and species separation dynamics of some symmetric binary LJ clusters, i.e., LJ clusters composed of a 50:50 mixture of two kinds of atom of equal size.

A common assumption in the computer-simulation studies performed so far on binary LJ clusters is that the collision diameters $\sigma_{\alpha\beta}$ of the interaction potentials are additive, i.e., $\sigma_{AB}=(\sigma_{AA}+\sigma_{BB})/2$. However, there is no compelling reason why this additivity should hold. In fact, nonadditivity has proved to be useful for interpreting several experimental results of bulk systems (see Ref. 9 and those quoted therein), and some authors have recently investigated the properties of bulk LJ (Ref. 10) and Yukawa[11] mixtures with nonadditive hard cores. Accordingly, it seems reasonable to study the properties of nonadditive LJ heteroclusters in order to gain insight into the behavior of small clusters containing more than one species of particle.

In this work, we carried out a MD study of the structure, melting, and ordering tendencies of some symmetric $A_{13}B_{13}$ LJ clusters with positive, zero, and negative nonadditivity; the zero-nonadditivity results extend those of Garzón *et al.*,[6] who used different values of the interaction parameters from those considered in this paper. For simplicity, we consider a model $A_{13}B_{13}$ LJ heterocluster consisting of two mechanically identical species, which are only differentiated by a label corresponding to some internal degree of freedom; the two species have the same mass and identical like-atom collision diameters and interaction strengths. In this idealized system, the effects of nonadditive collision diameters and of the unlike pairs interaction strength on the structure and phase behavior of the heterocluster stand out without being obscured by complicating factors such as, in particular, the particle size asymmetry that exists in real heteroclusters.

In Sec. II, we sketch the computational method used in this work, giving only such technical details as are strictly necessary. In Sec. III, we present and discuss our results on the structures, melting behavior, and ordering tendencies of additive and nonadditive $A_{13}B_{13}$ LJ clusters. Finally, in Sec. IV, we summarize the main conclusions of this work.

II. COMPUTATIONAL METHOD

We consider a binary cluster of $N=26$ particles containing $N_A=13$ atoms of species A and $N_B=13$ atoms of species B interacting pairwise through a LJ potential ϕ given by

$$\phi_{\alpha\beta}(r)=4\varepsilon_{\alpha\beta}\left[\left[\frac{\alpha_{\alpha\beta}}{r}\right]^{12}-\left[\frac{\sigma_{\alpha\beta}}{r}\right]^{6}\right], \tag{1}$$

where $\varepsilon_{\alpha\beta}$ and $\sigma_{\alpha\beta}$ ($\alpha,\beta=A,B$) are the well depth and the collision diameter for atoms of species α and β. The collision diameter of unlike species can be written as $\sigma_{AB}=(1+\Delta)(\sigma_{AA}+\sigma_{BB})/2$, where Δ is the nonadditivity parameter. As indicated above, in the calculations carried out in this work we assumed for simplicity that $\sigma_{AA}=\sigma_{BB}\equiv\sigma$ and $\varepsilon_{AA}=\varepsilon_{BB}\equiv\varepsilon$, so that each simulation is characterized by the values of $\Delta=(\sigma_{AB}/\sigma)-1$ and $\alpha\equiv\varepsilon_{AB}/\varepsilon$. Computations were performed using reduced units, namely, σ for length, ε for energy, $\tau\equiv(m\sigma^2/\varepsilon)^{1/2}$ for time, and $T^*\equiv KT/\varepsilon$ for temperature, where k is the Boltzmann constant and m is the mass of the particles. Constant energy MD simulations were carried out using the velocity Verlet algorithm[12] with a time step of $5\times10^{-3}\tau$, which guarantees conservation of the total energy of the cluster to within 0.001%. The center-of-mass momentum and the total angular momentum of the clus-

ter were eliminated from the calculations, so that the cluster temperature refers only to vibrational modes; it is given by[1]

$$T=\frac{2\langle E_{\rm kin}\rangle}{k(3N-6)}\ , \tag{2}$$

where $\langle E_{\rm kin}\rangle$ is the time-averaged kinetic energy of the cluster.

To obtain the lowest-energy structure of the binary cluster, an arbitrary starting configuration was propagated over 10^7 time steps, the atomic positions and velocities being recorded every 5×10^3 steps to obtain 2×10^3 uncorrelated configurations, to every one of which the steepest-descent method[13] was applied to find the corresponding local minimum. The energy of the 10^7-step trajectory was high enough to ensure appropriate sampling of the configuration space, but not so high as for particle evaporation to occur during the run. Repeating the process for several different starting configurations yielded some 10^3 different local-minimum energy structures for the heterocluster, but only a small number (those of lowest energy) were statistically important. To check the consistency of our results, the 100 configurations of lowest energy obtained for each value of α and Δ studied in this paper were taken as starting points for repetition of the steepest-descent method in search of possible new local-minimum energy structures for each other combination of values of α and Δ. However, no new local minima were found, suggesting that the structures reported in Sec. III for the various values of α and Δ very probably correspond to the global minima of the heteroclusters.

Starting from the $T=0$ ground-state configuration, the heterocluster was gradually heated in a stepwise manner to obtain the caloric curve, as indicated in Ref. 4. At each step, the state was allowed to propagate over 55×10^4 time steps, the first 5×10^4 for equilibration and the rest to obtain the corresponding caloric curve point by averaging the kinetic and potential energies. In the melting region, averages over longer times (up to 10^6 time steps) were used to smooth out the large thermodynamic fluctuations. To characterize phase changes in the cluster, we calculated the relative root-mean-square (rms) pair-separation fluctuation δ, given by[1]

$$\delta=\frac{2}{N(N-1)}\sum_{i<j}\frac{(\langle r_{ij}^2\rangle-\langle r_{ij}\rangle^2)^{1/2}}{\langle r_{ij}\rangle}\ , \tag{3}$$

as a function of temperature; and to throw light on the characteristics and ordering tendencies of the heterocluster at $T\neq0$, we also calculated, for each value of T, the average principal radii of gyration of the cluster ($\langle R_1\rangle$, $\langle R_2\rangle$, and $\langle R_3\rangle$) and the average separation between the centers of mass of the two species of particles, $\langle d\rangle$. The R_i are given by

$$R_i=\sqrt{I_i/N}\ , \tag{4}$$

and d by

$$d=|\mathbf{d}|=\left|\frac{\sum_{i=1}^{N_A}\mathbf{r}_i^{(A)}}{N_A}-\frac{\sum_{i=1}^{N_B}\mathbf{r}_i^{(B)}}{N_B}\right|\ , \tag{5}$$

where the I_i are the principal moments of inertia of the heterocluster and the $\mathbf{r}_i^{(A)}$ and $\mathbf{r}_i^{(B)}$ are the positions of the atoms of each species of particle.

III. RESULTS

A. Additive clusters

We first considered additive ($\Delta=0$) $A_{13}B_{13}$ LJ clusters with six values of the unlike pairs interaction strength parameter: $\alpha=0.5$, 0.8, 0.9, 1, 1.1, and 1.2. Values of α below unity favor demixing, and conversely for α above unity. The structural and dynamical properties of some larger additive LJ binary clusters with a demixing tendency have recently been studied by Clarke *et al.*[8]

The lowest-energy structures of the additive $A_{13}B_{13}$ LJ clusters, shown in Figs. 1 and 2, are based on icosahedral packing. These assignments, and those of the other clusters studied in this paper, were established by both checking the numerical values of the atomic coordinates and by computer-graphics visualization. The case $\alpha=1$ (Fig. 1) corresponds to the 26-atom pure LJ cluster, whose configuration can be considered as 4 interpenetrating 13-atom icosahedra, forming 6 double icosahedra.[14] The same ground-state configuration was obtained for $\alpha=0.9$ and 0.8, although the two species in the clusters are now segregated [Figs. 2(a) and 2(b)]. As indicated above, this mixing tendency is induced by the weak cross-interaction parameter α. For $\alpha=0.5$, the strong homocoordination tendency leads to a more elongated icosahedral configuration [Fig. 2(c)] formed by 2 13-atom icosahedra sharing an atom at 1 apex, with 1 extra atom outside the icosahedral core. The lowest-energy icosahedral structures for the cases $\alpha=1.1$ and 1.2, shown in Figs. 2(d) and 2(e), respectively, are similar to those for $\alpha=0.9$ and 0.8 except that, as a consequence of the tendency to heterocoordination which now exists, the two species are mingled rather than segregated.

Figure 3 shows the caloric curves calculated for the additive LJ heteroclusters considered above. As expected, for a given temperature, the larger the cross-interaction parameter α, the more negative is the total cluster energy. All the caloric curves present a change in slope

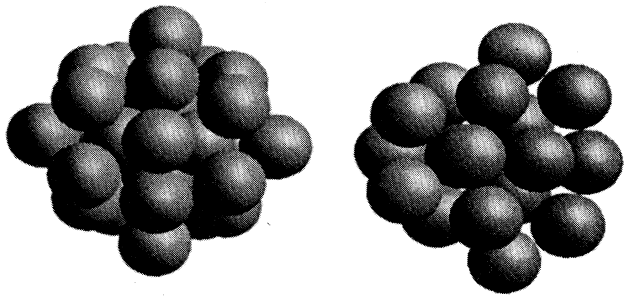

FIG. 1. Two mutually perpendicular views of the lowest-energy structure of the 26-atom pure LJ cluster. The right-hand view is the result of turning the left-hand view 90° to the left about an axis lying in the plane of the paper parallel to the vertical edges.

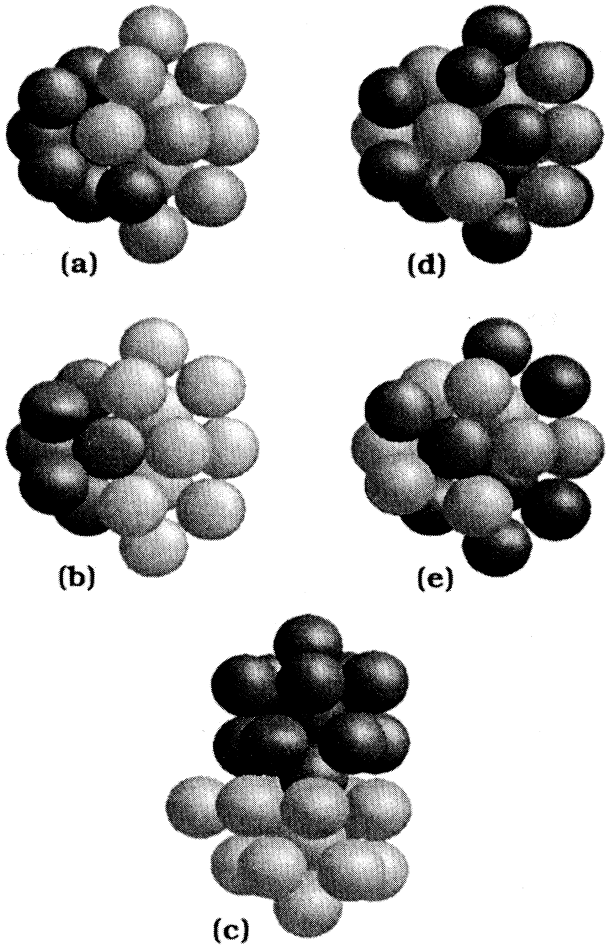

FIG. 2. The lowest-energy structures of the additive $A_{13}B_{13}$ LJ clusters with cross-interaction parameter $\alpha=0.9$ (a), 0.8 (b), 0.5 (c), 1.1 (d), and 1.2 (e).

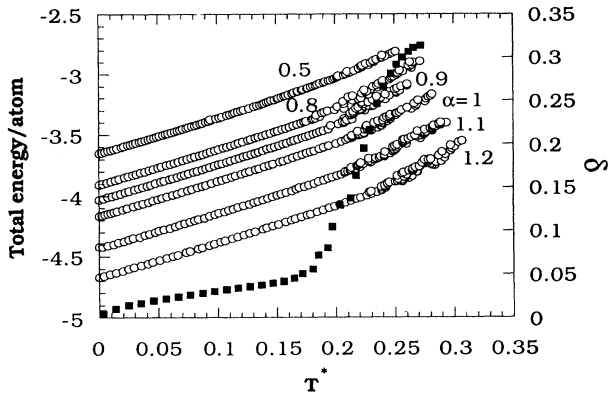

FIG. 3. Caloric curves for the additive $A_{13}B_{13}$ LJ cluster for several values of the cross-interaction parameter α. For $\alpha=1$, the system corresponds to the 26-atom pure LJ cluster. Open circles represent the total energy atom (in units of ε; left-hand scale), black squares the rms pair-separation fluctuations corresponding to the case $\alpha=0.8$ (right-hand scale).

reflecting the phase change from a rigid to a nonrigid structure. This transition is evidenced very clearly in Fig. 3 by the sharp increase in the rms pair-separation fluctuation δ for $\alpha=0.8$, shown by black squares. (The δ-T^* curves for the other values of α behaved similarly.) The melting temperatures of the clusters studied (calculated at $\delta=0.18$, which corresponds to the middle of the transition regions) are $T_m^*(\alpha=0.5)=0.21$, $T_m^*(\alpha=0.8)=0.22$, $T_m^*(\alpha=0.9)=0.22$, $T_m^*(\alpha=1)=0.24$, $T_m^*(\alpha=1.1)=0.25$, and $T_m^*(\alpha=1.2)=0.27$, which are all much smaller than the melting temperature of the bulk LJ pure system, $T_m^*\simeq 0.71$.[8] The uncertainty in these cluster melting temperatures can be estimated as about

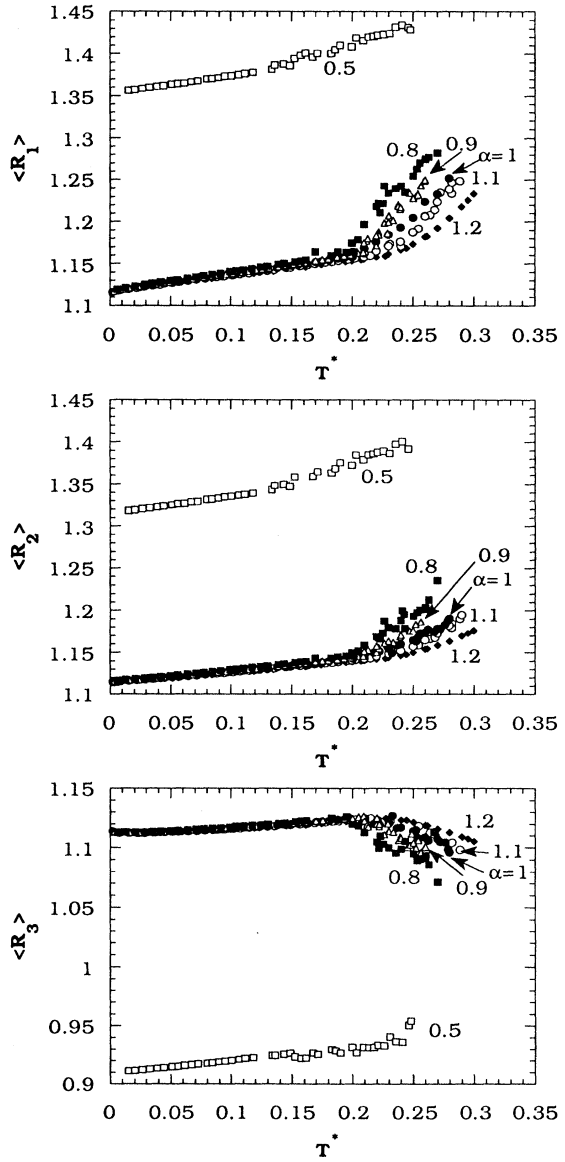

FIG. 4. Temperature dependence of the average principal radii of gyration (in units of σ) for the additive $A_{13}B_{13}$ LJ cluster, for several values of the parameter α. For $\alpha=1$, the system corresponds to the 26-atom pure LJ cluster.

$\pm 5\%$ from the uncertainties in the δ and T^* values obtained in our simulations.

Figure 4 shows the average principal radii of gyration as functions of temperature for the additive LJ binary clusters. At low temperatures there are few configurations accessible to the systems (just one in the $T=0$ ground states), as a result of which the fluctuations in $\langle R_1 \rangle$, $\langle R_2 \rangle$, and $\langle R_3 \rangle$ are small and all three radii increase with temperature as the cluster dilates. However, when the melting temperature is approached, fluctuations become larger, and it is only for $\alpha=0.5$ that all three radii of gyration continue to increase; for $\alpha=0.8$, 0.9, 1, 1.1, and 1.2, $\langle R_1 \rangle$ and $\langle R_2 \rangle$ increase but $\langle R_3 \rangle$ decreases markedly with increasing temperature. This means that within the melting region, the $\alpha=0.8$ to 1.2 clusters gain access to elongated configurations like that which is adopted by the $\alpha=0.5$ cluster even in the $T=0$ ground state [Fig. 2(c)].

Figure 5 shows, for each value of α of the additive heteroclusters, the calculated average separation between the centers of mass of the two species plotted as a function of temperature. The value $\langle d \rangle=0.5$ obtained in simulations for a fully mixed cluster ($\alpha=1$) is similar to the value obtained by Clarke *et al.*[8] for a fully mixed cluster with $N=110$. (*A* fully mixed A_nB_n cluster can be constructed by taking a $2n$-atom cluster and randomly labeling half of the particles *A* and the other half *B*.) Values of $\langle d \rangle$ above 0.5 indicate that there is a tendency to species separation, whereas values of $\langle d \rangle$ below 0.5 are indicative of a tendency to heterocoordination. For $\alpha=0.5$ and 0.8, the additive $A_{13}B_{13}$ LJ clusters exhibit species separation in the whole range of temperatures. For $\alpha=0.9$, however, the heterocluster shows species separation at low temperature [as we have already seen; Fig. 2(a)], but thermal agitation can mix the two species after melting. For $\alpha=1.1$ and 1.2, the two species are heterocoordinated at all temperatures.

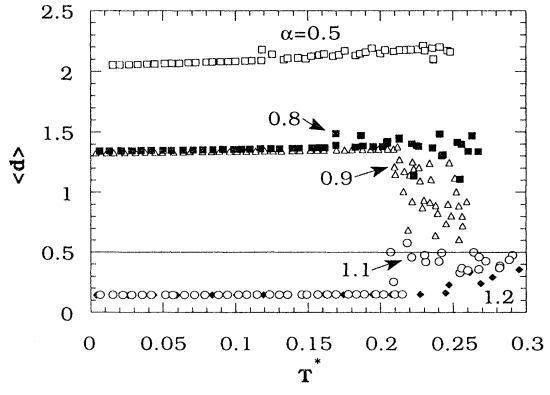

FIG. 5. Temperature dependence of the average separation between the centers of mass of the two species (in units of σ) for the additive $A_{13}B_{13}$ LJ cluster, for several values of the cross-interaction parameter α.

B. Nonadditive clusters

We investigated nonadditive $A_{13}B_{13}$ LJ clusters with $\alpha=1$ and $\Delta=0.1$, 0.2, -0.1, and -0.2. Small values of Δ have proved to be adequate for describing certain properties of bulk systems.[15] Values of $\Delta>0$ mean that the repulsion between unlike species is greater than that between like species, so that at low temperature, when the attractive interactions bring the atoms together, the atoms of each species tend to surround themselves with like atoms and avoid the other species. Thus, for $\Delta>0$ there is a tendency to species separation; conversely, for $\Delta<0$ there is a tendency to heterocoordination. The lowest-energy structures of the nonadditive clusters are shown in Fig. 6. For $\Delta=0.1$ and 0.2 [Figs. 6(a) and 6(b)] the clusters adopt distorted icosahedral configurations similar to those of Figs. 2(a) and 2(b), although due to the Δ values being quite small the clusters now show only partial demixing, forming single-species microdomains. For the negative values of the nonadditivity parameter [Figs. 6(c) and 6(d)], the systems are mixed clusters of the two species and no longer have icosahedral packing.

The calculated caloric curves for the LJ binary clusters with $\alpha=1$ all have the characteristic sigmoidal shape (Fig. 7). Both positive and negative nonadditivity produce clusters that are energetically more stable than the 26-atom pure LJ cluster (corresponding to $\Delta=0$). The cluster melting temperatures are similar to those of the additive cases considered above: $T_m^*(\Delta=0.1)=0.24$, $T_m^*(\Delta=0.2)=0.24$, $T_m^*(\Delta=-0.1)=0.23$, and $T_m^*(\Delta=-0.2)=0.19$.

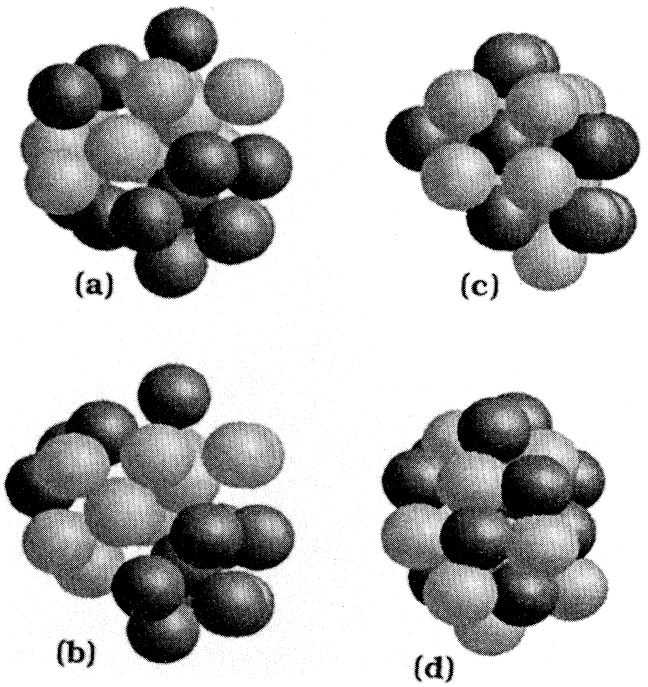

FIG. 6. The lowest-energy structures of the nonadditive $A_{13}B_{13}$ LJ clusters with nonadditivity parameter $\Delta=0.1$ (a), 0.2 (b), -0.1 (c), and -0.2 (d).

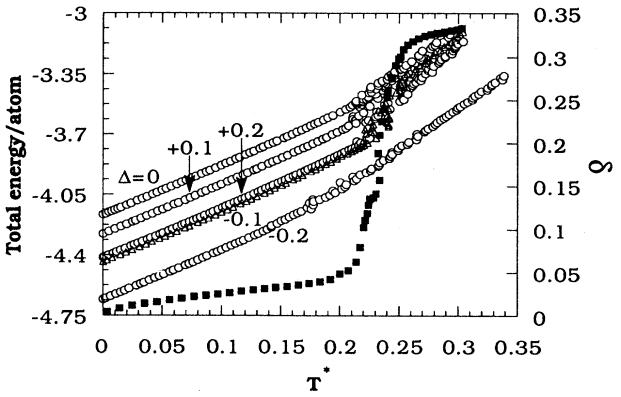

FIG. 7. Caloric curves for $A_{13}B_{13}$ LJ clusters with $\alpha=1$ and several values of the nonadditivity parameter Δ. Open symbols represent the total energy per atom (in units of ε; left-hand scale), black squares the rms pair-separation fluctuations corresponding to the case $\Delta=-0.1$ (right-hand scale).

Figure 8 shows the temperature dependence of $\langle R_1 \rangle$, $\langle R_2 \rangle$, and $\langle R_3 \rangle$ for the LJ heteroclusters with $\alpha=1$. As before, the dilation of these clusters with temperature is reflected by an increase in the average values of the principal radii of gyration. However, in the case $\Delta=-0.2$, there is a sharp decrease in $\langle R_2 \rangle$ and increase in $\langle R_3 \rangle$ at about $T^*=0.15$. By computer-graphics visualization, we established that these changes correspond to a structural change from an initial configuration that fluctuates around the nonicosahedral structure of Fig. 6(d) to a somewhat different configuration. The calculated $\langle R_i \rangle$ values indicate that clusters with $\Delta>0$ are more voluminous than the one-component ($\Delta=0$) cluster, and conversely for the clusters with $\Delta<0$. Finally, the temperature dependence of the average separation $\langle d \rangle$ between the centers of mass of the two species (Fig. 9) confirms that the clusters with $\Delta<0$ always exhibit a tendency to heterocoordination, and that the partially species-separated states of the clusters with $\Delta>0$ evolve to mixed states when thermal agitation causes melting. (Note, however, that the corresponding $\langle d \rangle$ values are never far above 0.5 before melting.)

IV. SUMMARY AND CONCLUSION

In this work we studied the characteristics of $A_{13}B_{13}$ LJ heteroclusters with additive and nonadditive collision diameters. For simplicity, we considered that the like-atom collision diameters and interaction strengths of the two species have the same value. The lowest-energy structures of the additive binary clusters studied are icosahedral, in keeping with the recent findings of Clarke *et al.*[8] for some larger LJ heteroclusters. Like pure LJ clusters,[1–5] the additive LJ heteroclusters melt at temperatures much lower than the melting temperature of the bulk pure LJ system. In this respect, the behavior of LJ clusters differs from that of certain single-metal clusters.[16] The $A_{13}B_{13}$ LJ heteroclusters with weakly nonad-

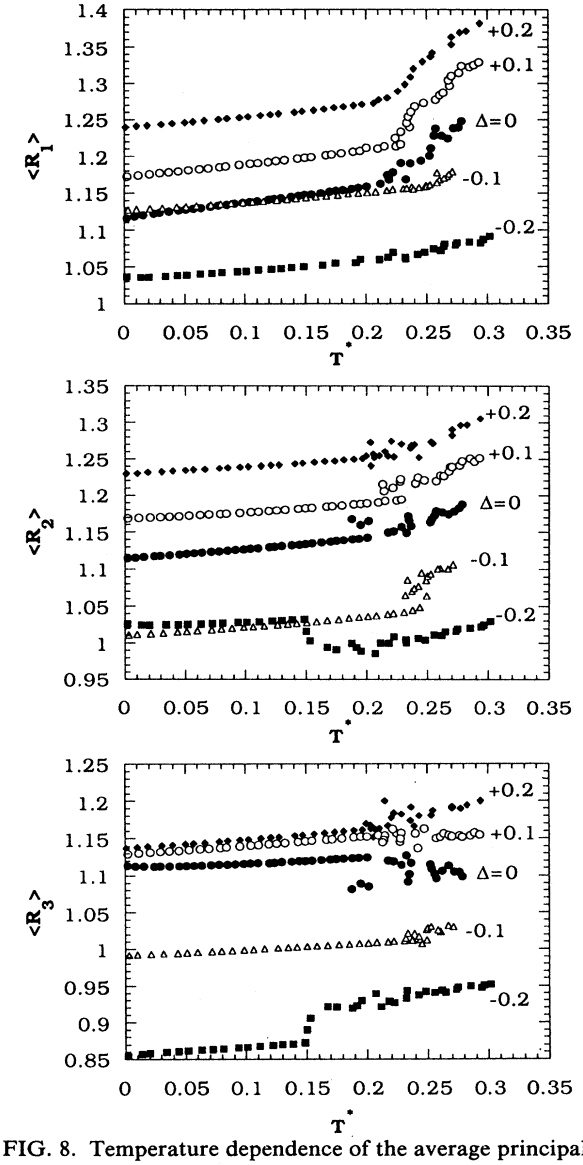

FIG. 8. Temperature dependence of the average principal radii of gyration of $A_{13}B_{13}$ LJ clusters with $\alpha=1$ and several values of the nonadditivity parameter Δ.

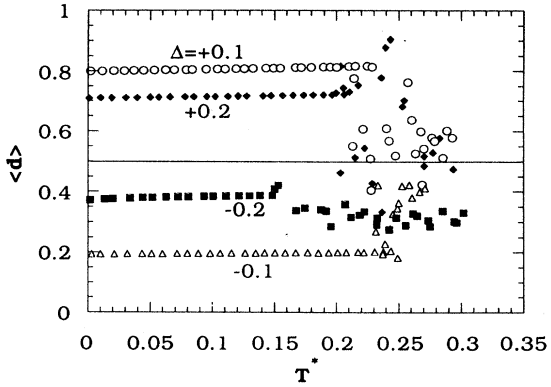

FIG. 9. Temperature dependence of the average separation between the centers of mass of the two species (in units of σ) for $A_{13}B_{13}$ LJ clusters with $\alpha=1$ and several values of the nonadditivity parameter Δ.

ditive collision diameters ($\Delta = \pm 0.1, \pm 0.2$) have melting temperatures similar to those of the additive clusters. Those with small positive nonadditivity have distorted icosahedral $T=0$ ground-state configurations, those with small negative nonadditivity are not icosahedral. Finally, the tendency to mixing or demixing of the additive $A_{13}B_{13}$ LJ clusters studied is directly correlated with the relative strength of unlike pair interactions, and that of the nonadditive clusters with the sign of the nonadditivity parameter, though demixing tendencies may be modified at high temperature due to thermal agitation.

Nonadditivity in the collision diameters can, therefore, have a significant effect on certain properties of LJ heteroclusters. Although the system considered here is an idealized $A_{13}B_{13}$ LJ heterocluster in which A and B have identical size and like-atom attraction strengths, it is expected that these results will be generalizable to more complex heteroclusters with size mismatch and with nonadditivities in the repulsive parts of the pair interactions.

ACKNOWLEDGMENTS

This work was supported by the DGICYT, Spain (Project No. PB92-0645-C03-03) and the Xunta de Galicia (Project No. XUGA20602B92). The authors are grateful to M. J. Grimson for useful comments.

[1] J. Jellinek, T. L. Beck, and R. S. Berry, J. Chem. Phys. **84**, 2783 (1986).
[2] H. L. Davis, J. Jellinek, and R. S. Berry, J. Chem. Phys. **86**, 6456 (1987).
[3] T. L. Beck, J. Jellinek, and R. S. Berry, J. Chem. Phys. **87**, 545 (1987).
[4] I. L. Garzón, M. Avalos-Borja, and E. Blaisten-Barojas, Phys. Rev. B **40**, 4749 (1989).
[5] D. J. Wales and R. S. Berry, J. Chem. Phys. **92**, 4283 (1990).
[6] I. L. Garzón, X. P. Long, R. Kawai, and J. H. Weare, Z. Phys. D **12**, 81 (1989).
[7] M. J. Grimson, Mol. Phys. **77**, 797 (1992).
[8] A. S. Clarke, R. Kapral, B. Moore, G. Patey, and X.-G. Wu, Phys. Rev. Lett. **70**, 3283 (1993).
[9] J. Jung, M. Jhon, and F. H. Ree, J. Chem. Phys. **100**, 528 (1994).
[10] H. M. Schaink and C. Hoheisel, J. Chem. Phys. **97**, 8561 (1992).
[11] C. Rey, L. E. González, L. J. Gallego, and D. J. González, J. Chem. Phys. **100**, 560 (1994).
[12] W. C. Swope, H. C. Andersen, P. H. Berens, and K. R. Wilson, J. Chem. Phys. **76**, 637 (1982).
[13] F. H. Stillinger and T. A. Weber, Phys. Rev. A **25**, 978 (1982).
[14] J. Farges, M. F. de Feraudy, B. Raoult, and G. Torchet, Surf. Sci. **156**, 370 (1985).
[15] D. Gazzillo and G. Pastore, Chem. Phys. Lett. **159**, 388 (1989).
[16] J. García-Rodeja, C. Rey, L. J. Gallego, and J. A. Alonso, Phys. Rev. B **49**, 8495 (1994).

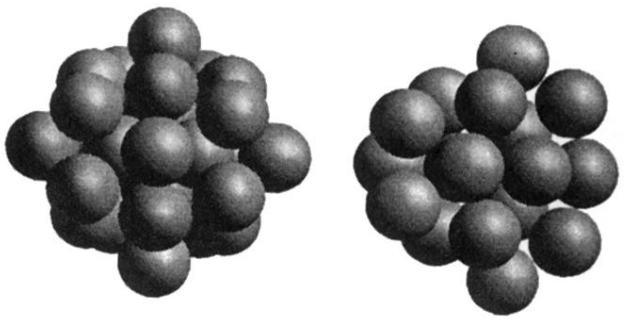

FIG. 1. Two mutually perpendicular views of the lowest-energy structure of the 26-atom pure LJ cluster. The right-hand view is the result of turning the left-hand view 90° to the left about an axis lying in the plane of the paper parallel to the vertical edges.

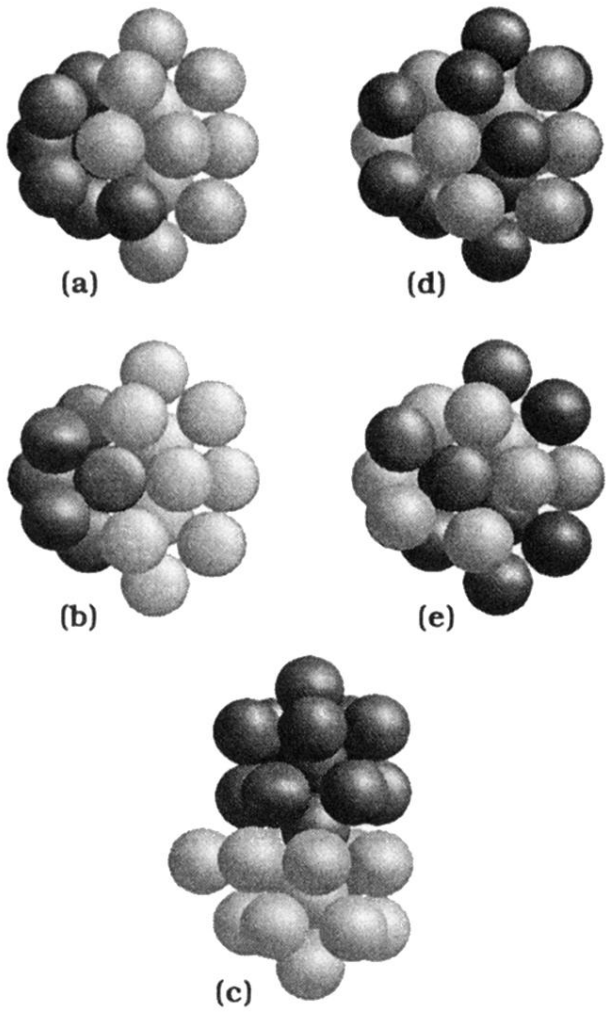

FIG. 2. The lowest-energy structures of the additive $A_{13}B_{13}$ LJ clusters with cross-interaction parameter $\alpha=0.9$ (a), 0.8 (b), 0.5 (c), 1.1 (d), and 1.2 (e).

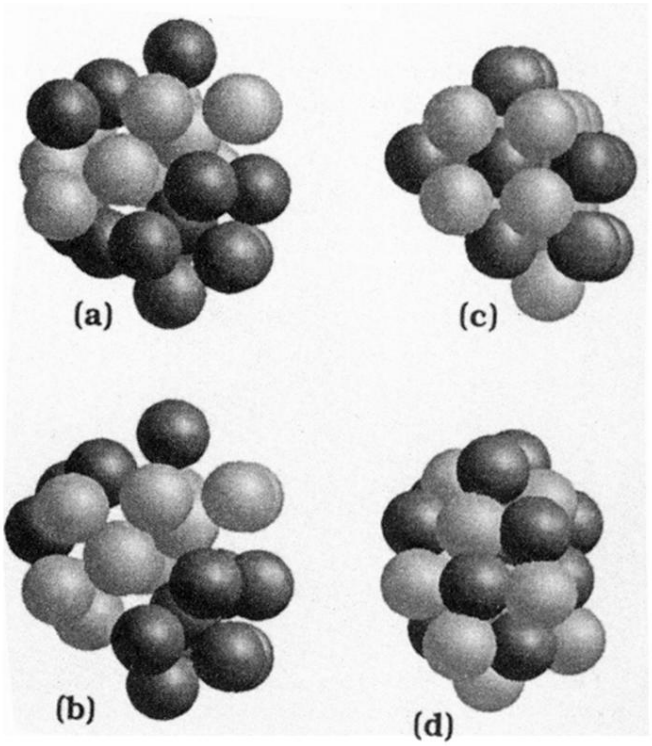

FIG. 6. The lowest-energy structures of the nonadditive $A_{13}B_{13}$ LJ clusters with nonadditivity parameter $\Delta = 0.1$ (a), 0.2 (b), -0.1 (c), and -0.2 (d).